### CONFERENCE PRE-PRINT

# EFFECTS OF ZONAL FIELDS ON ENERGETIC-PARTICLE EXCITATIONS OF REVERSED-SHEAR ALFVÉN EIGENMODES

L. Chen<sup>1,2</sup>, P.F. Liu<sup>3</sup>, R.R. Ma<sup>4,2</sup>, Z.H. Lin<sup>5</sup>, Z.Y. Qiu<sup>6,2</sup>, W.H. Wang<sup>5</sup> and F. Zonca<sup>2,1</sup>

<sup>1</sup>Institute for Fusion Theory and Simulation and School of Physics, Zhejiang University, Hangzhou 310027, China

<sup>2</sup>Center for Nonlinear Plasma Science and C.R. ENEA Frascati, C.P. 65, 00044 Frascati, Italy

<sup>3</sup>Beijing National Laboratory for Condensed Matter Physics, CAS Key Laboratory of Soft Matter Physics, Institute of Physics, Chinese Academy of Sciences, Beijing 100190, China <sup>4</sup>Southwestern Institute of Physics, PO Box 432, Chengdu 610041, China

<sup>5</sup>Department of Physics and Astronomy, University of California, Irvine, CA 92697-4574, United States of America

<sup>6</sup>Institute of Plasma Physics, Chinese Academy of Sciences (ASIPP), Hefei 230031, China

Corresponding Author: rrma@swip.ac.cn

#### Abstract:

Employing nonlinear gyrokinetic simulations and analytical theory, we investigate the effects of zonal (electromagnetic) fields (ZFs) on the saturation dynamics of reversed-shear Alfvén eigenmodes (RSAEs) driven by energetic particles (EPs) in tokamak plasmas. The key findings reveal that ZFs, generated through beat-driven RSAEs, influence mode saturation via two primary routes. One route involves the modification of EP dynamics by ZFs. Contrary to conventional expectations, simulations show that ZFs enhance the EP drive by modifying the EP phase-space zonal structure (PSZS), leading to higher saturation levels. These puzzling simulation results can be understood analytically in terms of the general fishbone-like dispersion relation with the correspondingly different EP-PSZS formations induced by ZFs. The other route involves the nonlinear dynamics of thermal plasmas. Simulations show that beat-driven ZFs can suppress RSAEs by inducing a net downward frequency shift. This shift results from competing effects: zonal flow induces an upward frequency chirping, while zonal current dominates to produce a net downward frequency chirping. The downward frequency shift enhances coupling to kinetic Alfvén waves (KAWs), triggering their outward propagating and the associated convective (radiative) damping, which ultimately saturates the mode. Numerical solutions of the eigenmode equation developed in this work confirm this tendency.

#### 1. Introduction

The interaction between energetic particles (EPs) and Alfvén eigenmodes (AEs) plays a critical role in determing the stability and transport properties of magnetically confined fusion plasmas. Among these modes, reversed-shear Alfvén eigenmodes (RSAEs) [1, 2] exhibit particularly complex dynamics due to their strong dependence on safety factor (q) profiles and enhanced coupling to EPs in reversed magnetic shear configurations. Such configurations are essential for achieving self-sustained, steady-state operations necessary for continuous fusion reactions. Recent nonlinear simulations [3, 4, 5] have demonstrated that zonal electromagnetic fields (ZFs) can be excited by RSAEs through beat-driven

mechanisms, leading to a significant reduction in the RSAE saturation level. The suppression of RSAEs by ZFs is known to occur through two primary routes: (i) nonlinear modifications to the dynamics of thermal plasmas, such as shifts in the mode frequency or modifications to the local current and safety factor profiles that enhance continuum damping [6], and (ii) modulation of EP phase-space dynmaics, altering their resonant interaction with RSAEs. However, the underlying physics of these mechanisms remains incompletely understood, with most studies offering only qualitative descriptions.

This work systematically investigates how ZFs affect the RSAE saturation via the dynamics of both EPs and thermal plasmas, by combining first-principles gyrokinetic simulations with analytical theory. Specifically, we address two observations: (1) contrary to conventional expectations of ZF stabilization, ZFs enhance the EP drive by modifying the PSZS of EPs; and (2) a downward frequency chirping, dominated by the zonal current, trigges mode conversion to KAWs and the associated convective damping, ultimately leading to saturation. Our results provide a unified theoretical framework for predicting AE saturation in burning plasmas.

#### 2. Simulation Model

We employ the gyrokinetic toroidal code (GTC) [7] to simulate RSAE dynamics with the equilibrium and plasma profiles are selected from DIII-D discharge #159243 [8]. The simulations employ a typical reversed magnetic shear configuration with minimal safety factor  $q_{\min} = 2.94$  near major radius R = 1.98 m on the mid-plane for the low field side, where RSAE are observed in experiments and validated in simulations. Here, q, the safety factor, represents the ratio of toroidal to poloidal turns of magnetic field lines.

For the GTC simulation model [9], EP and thermal ions are described by gyrokinetic model [10], and electrons are described by drift kinetic model. Since  $\beta \ll 1$  and  $nq \gg 1$ , the effects of compressible magnetic perturbation  $\delta B_{\parallel}$  and equilibrium current  $J_{\parallel 0}$  on RSAE, as verified in previous simulations, are negligible. Here  $\beta$  is the ratio between plasma and magnetic pressures, and n is the toroidal mode number. Using the parallel simplistic description [10], the perturbed gyrokinetic Vlasov equation can be written as

$$(\mathcal{L}_0 + \delta \mathcal{L})\delta F = -\delta \mathcal{L}F_0, \tag{1}$$

where  $F_0$  is the equilibrium distribution,  $\delta F$  is the perturbed distribution, and the equilibrium and perturbed propagators in the  $(\mathbf{X}, v_{\parallel})$  phase space are given, respectively, by

$$\mathcal{L}_{0} = \frac{\partial}{\partial t} + \left( \upsilon_{\parallel} \boldsymbol{b}_{0} + \boldsymbol{v}_{d} \right) \cdot \frac{\partial}{\partial \boldsymbol{X}} - \frac{\mu \boldsymbol{B}_{0}^{*}}{B_{0}} \cdot \nabla B_{0} \frac{\partial}{\partial \upsilon_{\parallel}}, \tag{2}$$

and

$$\delta \mathcal{L} = \left( \boldsymbol{v}_E + \frac{v_{\parallel} \delta \boldsymbol{B}_{\perp}}{B_0} \right) \cdot \frac{\partial}{\partial \boldsymbol{X}} - \left( \frac{\mu \delta \boldsymbol{B}_{\perp} \cdot \nabla B_0}{B_0} + Z \frac{\boldsymbol{B}_0^*}{m B_0} \cdot \nabla \delta \phi + \frac{Z}{cm} \frac{\partial \delta A_{\parallel}}{\partial t} \right) \frac{\partial}{\partial v_{\parallel}}. \tag{3}$$

Here,  $\boldsymbol{X}$  is the gyro-center position,  $v_{\parallel}$  is the parallel velocity,  $\mu = v_{\perp}^2/2B_0$  is the magnetic momentum, Z is the particle charge, m is the particle mass, c is the light speed,  $\boldsymbol{B}_0$  is the equilibrium magnetic field,  $\delta \boldsymbol{B}_{\perp}$  is the perpendicular magnetic perturbation,  $\delta A_{\parallel}$  is the parallel component of vector potential, and  $\delta \phi$  is the scalar potential. Furthermore,  $\boldsymbol{v}_d = \boldsymbol{b}_0 \times \left(\mu \boldsymbol{\nabla} B_0 + v_{\parallel}^2 \boldsymbol{\kappa}\right)/\Omega$ ,  $\boldsymbol{v}_E = \frac{c}{B_0} \boldsymbol{b}_0 \times \nabla \delta \phi$ ,  $\boldsymbol{B}_0^* = \boldsymbol{B}_0 + \frac{B_0 v_{\parallel}}{\Omega} \boldsymbol{b}_0 \times \boldsymbol{\kappa}$ , where  $\boldsymbol{b}_0 = \boldsymbol{B}_0/B_0$ ,  $\Omega = ZB_0/mc$ , and  $\boldsymbol{\kappa} = (\boldsymbol{b}_0 \cdot \boldsymbol{\nabla})\boldsymbol{b}_0$  being the curvature of  $\boldsymbol{B}_0$ . For a single n mode simulation with zonal components (labeled as subscript "z"), Eq. 1 can be further written

as,

$$(\mathcal{L}_0 + \delta \mathcal{L}_n + \delta \mathcal{L}_z) \left( \delta F_n + \delta F_z \right) = -\left( \delta \mathcal{L}_n + \delta \mathcal{L}_z \right) F_0, \tag{4}$$

where  $\mathcal{L}_n$  and  $\mathcal{L}_z$  correspond to the perturbed propagators, Eq. 3, with, respectively, the toroidal mode number n and zonal components of the electromagnetic fields.

In GTC simulations, an initial Maxwellian distribution is used for thermal plasmas and EP with  $T_e = T_i = 1$  keV and  $T_E = 20$  keV. Simulations are performed using a low noise  $\delta f$  scheme [11] with a particle number per cell 1000 to minimize the noise. The radial boundary of the simulation domain is R = [1.81, 2.23] m. Based on the convergence studies, GTC uses a global field-aligned mesh with 32 parallel grid points, which is sufficient to resolve the long parallel wavelength, and  $5 \times 10^4$  unstructured perpendicular grid points with a grid size  $\sim 1.3\rho_i$  to capture the finite Lamor radius effect, where  $\rho_i \sim 2.1$  mm is the thermal ion gyroradius. Time step is set to be  $2 \times 10^{-5}$  ms to resolve the high frequency RSAE and the fast electron thermal motion  $v_{th,e} \sim 2 \times 10^7$  m/s. In addition, the initial condition is only random noise, and all poloidal harmonics are included for a select specific toroidal mode using Fourier filtering.

# 3. ZF effects on RSAE via EP dynamics

In order to delineate the effects of zonal fields  $(\delta \phi_z, \delta A_{\parallel z})$  on the EP dynamics, three cases of simulations, labeled as Case A, B, and C, are carried out for the most unstable n=4 RSAE. Case A corresponds to the No-ZFs case, where we set  $\delta \mathcal{L}_z=0$  in the EP gyrokinetic Vlasov equation, Eq. 4, in order to remove the effects of ZFs on EP. Case B corresponds to the Full-ZFs case, where  $\delta \mathcal{L}_z$  on both sides of Eq. 4 is kept for EP. Meanwhile, Case C corresponds to the Partial-ZFs case, where we keep  $\delta \mathcal{L}_z$  in the right-hand side of Eq. 4; but we set  $\delta \mathcal{L}_z=0$  in the left-hand side of Eq. 4, i.e., the EP perturbed propagator, in order to remove the so-called shearing effects due to ZFs. Note that, in all three cases, ZFs are fully kept for the thermal electrons and ions.

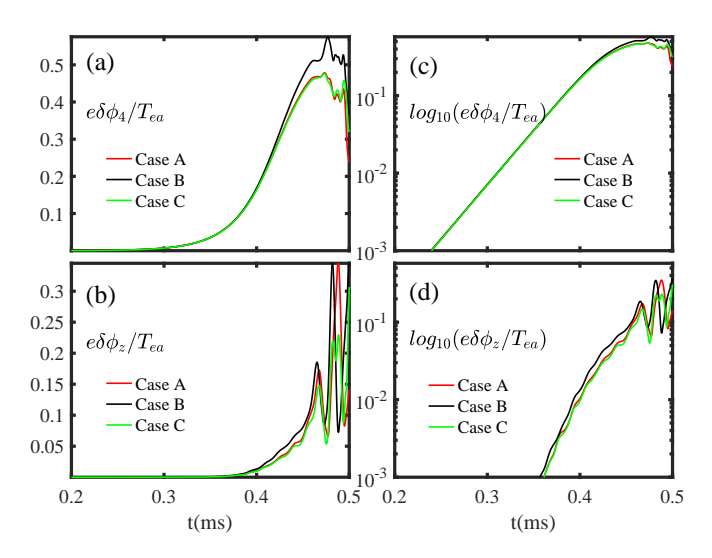


FIG. 1: Time history of perturbed electrostatic potential  $e\delta\phi_4/T_{ea}$  (panel a), normalized by the on-axis electron temperature  $T_{ea}$ , for the selected toroidal n=4 modes on  $q_{min}$  flux surface from Case A (red), B (black) and C (green). The normalized zonal scalar potential  $e\delta\phi_z/T_{ea}$  (panel b) is the root-mean-square (rms) value averaged over the radial domain of the major radius R=[1.91,2.04] m. Panel (c) and (d) are the corresponding plots using a base-10 logarithmic scale on the vertical axis.

Figure 1 (a) shows the time history of mode amplitude of n = 4 RSAE scalar potential,

 $\delta\phi_4$ , for the three simulation cases. In the early linear phase, i.e., before 0.4 ms, effects of ZFs on the RSAE amplitude are negligible due to the small amplitude of ZFs. However, in the later linear phase, the Full-ZFs Case B, exhibits a stronger drive and, thereby, a higher initial saturation level than the No-ZFs Case A and Partial-ZFs Case C. This result is surprising; since it contradicts with the conventional expectation that ZFs tend to suppress instabilities. Furthermore, that the No-ZFs Case A essentially overlaps with the Partial-ZFs Case C is also puzzling; since it suggests that  $\delta \mathcal{L}_z$  in the right-hand side of Eq. 4 has a negligible effect on RSAE excitations by EP. It is worthwhile noting that the effects of ZFs also enter implicitly via the PSZS,  $\delta F_z$ , which cannot be suppressed in simulations. Consequently, these seemingly surprising and puzzling simulation results could be understood analytically in terms of the different EP PSZS nonlinearly generated in the three cases, which has been well documented in Ref. [12]. Figure 1 (b), meanwhile, plots the time history of the nonlinearly generated zonal potentials,  $\delta \phi_z$ , for the three cases. Curves for  $e\delta\phi_4/T_{ea}$  and  $e\delta\phi_z/T_{ea}$  are also plotted in Figs. 1 (c) and (d) in semi-log scale. During the linear phase, it is observed, as in previous RSAE simulations, that the ZFs grow at twice the linear growth rate of RSAE; clearly indicating that the ZFs are beat driven by RSAE [3, 5, 13]. The corresponding time histories of the parallel vector potential,  $\delta A_{\parallel}$  are not shown here presenting the same features as  $\delta \phi$ .

Adopting the beat driven generating mechanism, we have derived the corresponding analytical expressions of  $\delta\phi_z$  and  $\delta A_{\parallel,z}$  by considering a large aspect-ratio tokamak with circular magnetic surfaces; i.e.,  $\epsilon \equiv r/R \sim \mathcal{O}(10^{-1}) < 1$  with r and R being, respectively, the minor and major radii.  $\beta$ , meanwhile, is taken to be  $\mathcal{O}(\epsilon^2) \ll 1$ . Let  $\Omega_0 = (\omega_0, n_0)$  denotes a RSAE with toroidal mode number  $n_0$  and mode frequency  $\omega_0 = \omega_{0r} + i\partial_t$ . Note  $\Omega_0$  could be either linearly excited by EPs with  $\partial_t = \gamma_0 \ll \omega_{0r}$  being the linear growth rate, or excited by an external antenna with  $\partial_t \to 0^+$ . Since  $\beta \ll 1$ , magnetic compression is negligible and, thus,  $\Omega_0$  is described by electromagnetic perturbations;  $\delta\phi_0$  and  $\delta A_{\parallel 0}$  with  $\delta\phi_0$  and  $\delta A_{\parallel 0}$  being the scalar and parallel vector potentials, respectively. More specifically, we take

$$\begin{pmatrix} \delta \phi_0 \\ \delta A_{\parallel 0} \end{pmatrix} = e^{-i\omega_{0r}t + in_0\xi} \sum_m \begin{pmatrix} \Phi_m(r,t) \\ A_m(r,t) \end{pmatrix} e^{-im\theta} + \text{c.c.}$$
 (5)

Here,  $\xi$  is the toroidal angle and  $\theta$  the poloidal angle. Since  $|k_{\perp 0}\rho_i|^2 \ll 1$  with  $k_{\perp 0}$  being the perpendicular wave vector for  $\Omega_0$ , we may further assume  $\Omega_0$  satisfying the ideal MHD approximation;  $\delta E_{\parallel 0} \simeq 0$ ; i.e.,  $\omega_0 \delta A_{\parallel 0} = -ic(\boldsymbol{b}_0 \cdot \nabla)\delta\phi_0$ , or  $k_{\parallel m}\Phi_m = \omega_0 A_m/c$ ,  $k_{\parallel m} = (n_0 q - m)/qR$ .

We now consider the nonlinear generation of the zero-frequency ZFs beat driven by  $\Omega_0$ . Let the corresponding zonal state be denoted as  $\Omega_z = (\omega_z, n = 0)$ ; that is,

$$\begin{pmatrix} \delta \phi_z \\ \delta A_{\parallel z} \end{pmatrix} = \begin{pmatrix} \Phi_z(r,t) \\ A_z(r,t) \end{pmatrix} + \text{c.c.}, \tag{6}$$

and  $|-i\omega_z| = |\partial_t \ln \Phi_z| = |\partial_t \ln A_z| \ll \omega_{bi}$ ,  $\omega_{ti}$ ,  $\omega_{0r}$  with  $\omega_{bi}$  and  $\omega_{ti}$  being, respectively, the thermal ion bounce and transit frequencies. The governing equations for the ZF generation are derived from the nonlinear gyrokinetic equation [14], the quasi-neutrality condition, and the parallel Ampère's law equation. A detailed derivation can be found in

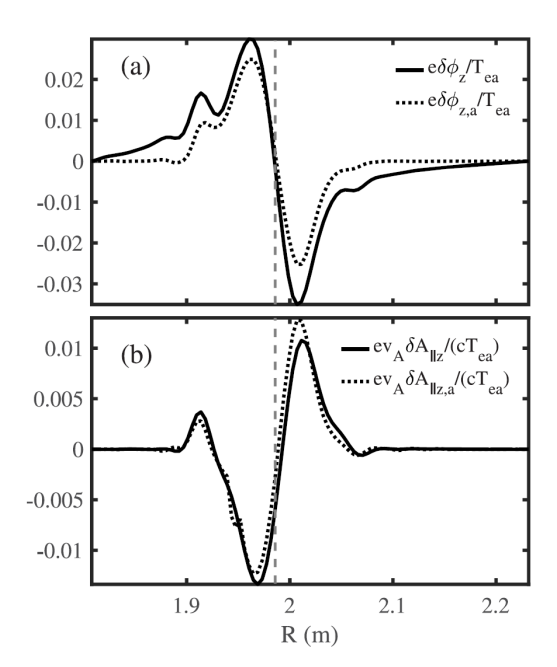


FIG. 2: Radial profiles of normalized zonal scalar potential  $\delta \phi_z$  from the Full-ZFs Case B (solid line) and the analytically derived  $\delta \phi_z$  using Eq. 8 with  $c_0 = 1$  (dot dash line) on the mid-plane for the low field side at t = 0.42 ms [panel (a)]. The radial profiles of corresponding normalized zonal parallel vector potential  $\delta A_{\parallel z}$  using Eq. 7 are shown in panel (b). The gray dash lines represent the  $q_{min}$  flux surface.

Ref. [12]; here we present the final results:

$$\frac{A_z}{c} \simeq \frac{c}{B_0 \omega_{0r}^2} \frac{\partial}{\partial r} \left[ k_{\theta 0} k_{\parallel 0} |\delta \phi_0|^2 \right]. \tag{7}$$

and

$$\Phi_z \simeq \frac{c}{B_0} \frac{1}{\omega_{0r}^2} (1 + c_0 \eta_i) \partial_r \left[ k_{\theta 0} \omega_{*in} |\delta \phi_0|^2 \right]. \tag{8}$$

where  $c_0 = \langle (1 - \mathcal{J}_{z_0}^2)(v^2/2v_{ti}^2 - 3/2)F_{Mi}\rangle_v/\langle (1 - \mathcal{J}_{z_0}^2)F_{Mi}\rangle_v$  corresponds to the Rosenbluth-Hinton neoclassical polarization due to the trapped ions [15]. Equations 7 and 8, thus, correspond to the zonal electromagnetic fields, ZFs, beat driven by the ponderomotive force of the RSAE,  $\Omega_0$ .

To compare the analytical expression with simulation results, we have plotted (black solid line) in Fig. 2 (a) the radial profile of normalized  $\delta \phi_z$  from the Full-ZFs Case B simulation at t=0.42 ms linear phase. The black dash line, meanwhile, is the corresponding analytical curve according to Eq. 8 with  $c_0=1$ . Similar curves for  $\delta A_{\parallel z}$  with Eq. 7 are plotted in Fig. 2 (b). It can be observed that the analytical and simulation results are in good agreement for both zonal fields.

To analyze how ZFs affect the EP drive on RSAEs, a corresponding analytical theory was also developed in Ref. [12]. The theory is discussed in detail and demonstrates that, in each case, the ZF-induced EP PSZSs are different. According to the GFLDR, this difference gives rise to additional stabilization or destabilization by ZFs, which is consistent with the simulation results. In particular, ZFs tend to enhance EPs drive and thereby increase the RSAE saturation level. This implies that ZFs must suppress RSAE predominantly through nonlinear thermal plasma dynamics.

# 4. ZF effects on RSAE via thermal plasma dynamics

This section shifts the focus to the suppression of RSAE through ZFs effects on the thermal plasma nonlinearities. We perform simulations where EPs are treated linearly while retaining full nonlinear dynamics for thermal plasmas.

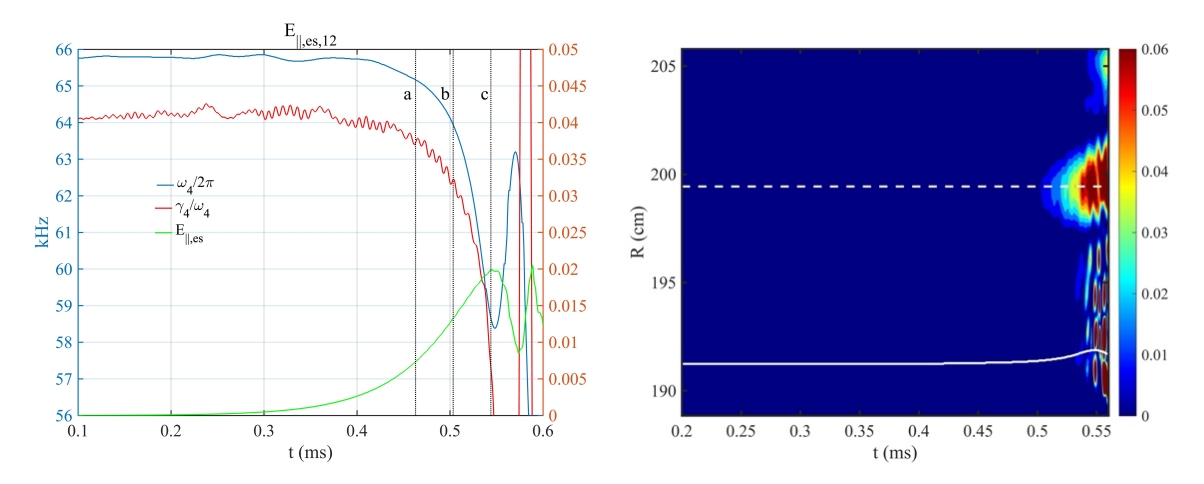


FIG. 3: (Left) Time evolution of RSAE frequency (blue), normalized growth rate (red), and amplitude of the parallel electrostatic field (green). (Right) Corresponding time-resolved radial profile of the parallel electric field. The white dashed line marks the  $q_{\min}$  surface, and the white solid line represents the Alfvén resonance.

GTC simulation results in Fig. 3 capture the key nonlinear saturation dynamics of the RSAE. The onset of downward frequency chirping (blue curve, left panel) coincides with a surge in the parallel electrostatic field  $E_{\parallel,es}$  (green curve) and a drop in the normalized growth rate  $\gamma_4/\omega_4$  (red curve) to near zero. This significant growth of  $E_{\parallel,es}$  provides evidence for the excitation of kinetic Alfvén waves (KAWs), pointing to a mode conversion from the large-scale RSAE. This conversion occurs when the RSAE frequency shifts downward toward the continuum spectrum at the  $q_{\min}$  surface, which enhances electron-ion decoupling and gives rise to a finite  $E_{\parallel,es}$ . The right panel confirms this interpretation, showing the subsequent outward propagation of the generated KAWs from the  $q_{\min}$  surface. The clear temporal correlation between RSAE saturation and the emergence of propagating KAWs strongly supports mode conversion as the underlying saturation mechanism.

To understand the nonlinear saturation of RSAEs observed in GTC simulations, we develop a comprehensive theoretical framework by self-consistently incorporating finite Larmor radius (FLR) effects and electron Landau damping dynamics. The resulting eigenmode equation, termed the "RSAE-KAW-e-Landau" model, is derived from the nonlinear gyrokinetic equation set. The influence of ZFs enters through three key nonlinear modifications: a nonlinear Ohms law, Maxwell stress, and Reynolds stress. The governing equation takes the form:

$$\rho_{i}^{2}\nabla_{\perp}^{2}\left(1 - \frac{\omega_{*pi}}{\omega}\right)\left[\frac{3}{4}\left(\omega^{2} - \omega_{\text{gam}}^{2}\right) + \frac{\tau k_{\parallel}^{2}v_{A}^{2}}{(1 - \omega_{*e}/\omega)(1 + \zeta_{e}Z(\zeta_{e}))}\right]\nabla_{\perp}^{2}\delta\phi_{0} + \nabla_{\perp}\cdot\epsilon_{A}\nabla_{\perp}\delta\phi_{0} + \Lambda\delta\phi_{0} + \nabla\cdot\left[\left(\nabla\alpha_{\phi2}\right)\delta\phi_{0}\right] = 0,$$
(9)

where  $\epsilon_A = \epsilon_{A0} + \alpha_{\phi 1} + \alpha_A$ ,  $\epsilon_{A0} = \left[ \left( 1 - \omega_{*pi}/\omega_0 \right) (\omega_0^2 - \omega_{\rm gam}^2) \right] - k_{\parallel 0}^2 v_A^2$ , and  $\omega_{\rm gam}^2 = (v_{ti}/R)^2 (\tau + 7/4)$  is the geodesic-acoustic frequency. The term  $\Lambda$  denotes effects such as

favorable average curvature, toroidal couplings, as well as wave-particle interactions due to thermal and energetic particles [18].  $\alpha_A = -2\frac{c}{B_0}\omega_0 k_{\theta 0}(\frac{k_{\parallel 0}v_A^2}{\omega_0 c}\delta A'_{\parallel z}), \ \alpha_{\phi 1} = \frac{c}{B_0}\omega_0 k_{\theta 0}(\frac{k_{\parallel 0}^2v_A^2}{\omega_0^2} + 1 - \frac{\omega_{*pi}}{\omega_0})\delta\phi'_z, \ \alpha_{\phi 2} = \frac{c}{B_0}\omega_0 k_{\theta 0}(\frac{k_{\parallel 0}^2v_A^2}{\omega_0^2} - 1 + \frac{\omega_{*pi}}{\omega_0})\delta\phi'_z.$  This model self-consistently describes RSAE-KAW coupling, with FLR terms removing the singularity at  $\epsilon_{A0} = 0$  and electron Landau damping enabling the description of radiative losses. In the limit where kinetic effects are neglected, the model reduces to the RSAE-MHD model.

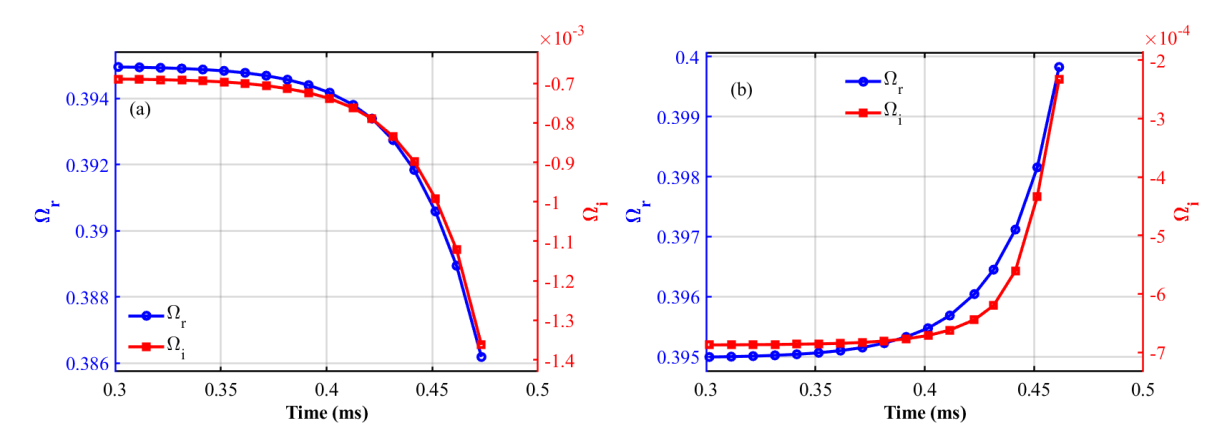


FIG. 4: Time evolution of the normalized frequency and damping rate of the RSAE within the "RSAE-MHD" model, in the presence of (a) both zonal flow and zonal current and (b) only zonal flow.

We first examine the respective roles of zonal flow and zonal current using the RSAE-MHD model. Figure 4 (a) presents the time evolution of the normalized frequency and damping rate when both zonal flow and zonal current are included. The results show distinct downward frequency chirping, consistent with GTC simulation results, while the nonlocal continuum damping remains exponentially small  $(10^{-4} \text{ to } 10^{-3})$  and increases gradually. In contrast, when zonal current is artificially removed (Fig. 4 (b)), the frequency chirps upward and the continuum damping decreases. This direct comparison confirms that zonal current dominates the downward chirping, whereas zonal flow alone drives upward chirping. We next analyze the RSAE-KAW-e-Landau model. As shown in

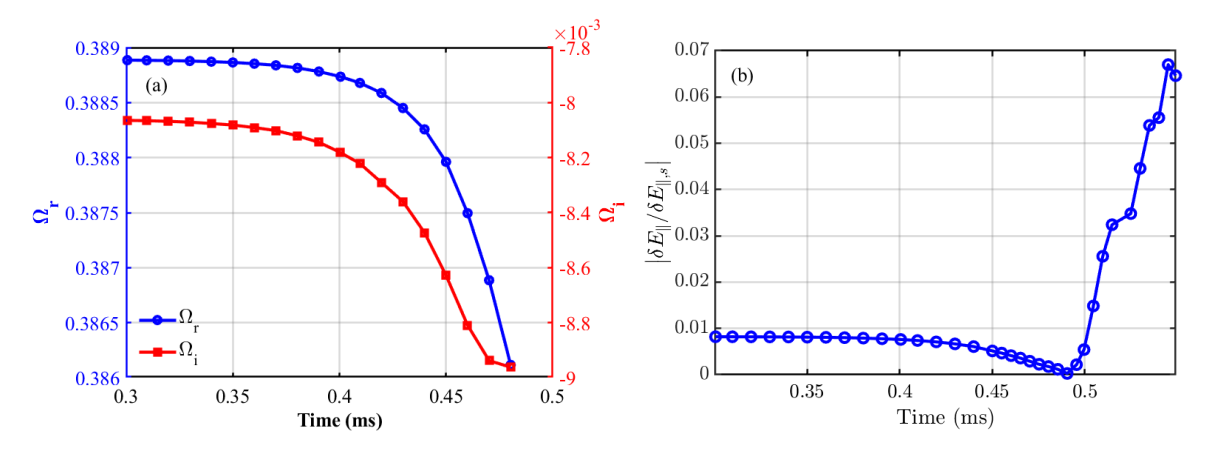


FIG. 5: (a) Time evolution of the normalized frequency and damping rate of the RSAE within the "RSAE-KAW-e-Landau" model, incorporating both zonal flow and zonal current. (b) Time evolution of the ratio  $|\delta E_{\parallel}/\delta E_{\parallel,es}|$ .

Fig. 5 (a), the frequency again exhibits downward chirping, but the radiative damping

rate is now one to two orders of magnitude larger than the MHD continuum damping. Figure 5 (b) shows a rapid increase in the ratio  $|\delta E_{\parallel}/\delta E_{\parallel,es}|$  after t=0.48 ms, signaling the excitation of KAWs and the enhancement of the parallel electric field  $\delta E_{\parallel}$ . This behavior, in excellent agreement with simulations, confirms that radiative damping via KAW conversion is the dominant saturation mechanism.

# 5. Discussion and Summary

This study investigates the dual routes through which zonal fields (ZFs) influence the nonlinear evolution of RSAEs, employing integrated gyrokinetic simulations and theoretical analysis. Our finding reveal that beat-driven ZFs modulate saturation through two distinct mechanisms: (i) modification of EP phase-space zonal structures (PSZS), which unexpectedly enhances the EP drive and elevates the saturation level; and (ii) thermal plasma dynamics, specifically, downward frequency chirping and mode conversion to kinetic Alfvén waves (KAWs), which suppress RSAEs via strong radiative damping. The paradoxical EP drive enhancement is explained theoretically via the generalized fishbone-like dispersion relation incorporating ZF-induced PSZS modifications. Meanwhile, ZF-induced frequency down-shifting triggers conversion to KAWs, establishing an effective saturation mechanism that quantitatively balances the EP drive. The excellent agreement between simulations and theoretical predictions confirms that although ZFs can amplify driving through PSZS effects, the dominant saturation route under typical conditions operates via thermal plasma dynamics, where KAW-mediated radiative damping effectively suppresses RSAE activity.

This work has been supported in part by the National key R&D Program of China under Grant No. 2022YFE03040002, the National Science Foundation of China under Grant Nos. 12175053, 12261131622 and 1205508, the Italian Ministry of Foreign Affairs with Grant No. CN23GR02, the Natural Science Foundation of Sichuan under Grant No. 2025ZNSFSC0064, the Strategic Priority Research Program of the Chinese Academy of Sciences (Grant No. XDB0500302), and the start-up funding of Institute of Physics, Chinese Academy of Sciences under Grant No. E3CB031R21, used computing resources at NERSC (DOE Contract DE-AC02-05CH11231).

# References

- [1] H. Kimura, et al. Nucl. Fusion 38, 1303 (1998).
- [2] S. E. Sharapov, et al. Phys. Lett. A 289, 127 (2001).
- [3] Y. Chen, et al. Phys. Plasmas 25, 032304 (2018).
- [4] T. Wang, et al. Plasma Sci. Technol. 26, 053001 (2024).
- [5] P. Liu, et al. Rev. Mod. Plasma Phys. 7, 15 (2023).
- [6] S. Wei, et al. J. Plasma Phys. 87, 905870505 (2021).
- [7] Z. Lin, et al. Science **281**, 3 (1998).
- [8] L.L. Lao, et al. Nucl. Fusion **25**, 1611 (1985).
- [9] I. Holod, et al. Phys. Plasmas 16, 122307 (2009).
- [10] A.J. Brizard, et al. Rev. Mod. Phys. 79, 421 (2007).
- [11] S.E. Parker, et al. Phys. Fluids B 5, 77 (1993).
- [12] L. Chen, et al. Nucl. Fusion 65, 016018 (2025).
- [13] T. Wang, et al. Nucl. Fusion **60**, 126032 (2020).
- [14] E.A. Frieman, et al. Phys. Fluids B 25, 502 (1982).
- [15] M.N. Rosenbluth, et al. Phys. Rev. Lett. 80, 724 (1998).
- [16] C.Z. Cheng, et al. Ann. Phys. **161**, 21 (1985).
- [17] L. Chen, et al. Rev. Mod. Phys. 88, 015008 (2016).
- [18] F. Zonca, et al. Phys. Plasmas 9, 4939 (2002).